AGU PUBLICATIONS

JGR

Journal of Geophysical Research: Earth Surface

RESEARCH ARTICLE

10.1002/2017JF004373

Can Seismic Observations of Bed Conditions on Ice Streams Help Constrain Parameters in Ice Flow Models?

Teresa M. Kyrke-Smith[1], **G. Hilmar Gudmundsson**[1], **and Patrick E. Farrell**[2]

[1]British Antarctic Survey, Cambridge, UK, [2]Mathematical Institute, University of Oxford, Oxford, UK

Key Points:
- We make new comparisons of ice sheet basal conditions estimated by two methods (model inversion versus seismic measurements)
- There is correlation between mean values of basal slipperiness and acoustic impedance when averaged over large enough length scales
- Seismic measurements of bed properties cannot be incorporated into models unless a physical theory is developed

Supporting Information:
- Supporting Information S1
- Figure S1
- Figure S2

Correspondence to:
T. M. Kyrke-Smith,
terkyr@bas.ac.uk

Citation:
Kyrke-Smith, T. M., Gudmundsson, G. H., & Farrell, P. E. (2017). Can seismic observations of bed conditions on ice streams help constrain parameters in ice flow models? *Journal of Geophysical Research: Earth Surface*, *122*, 2269–2282. https://doi.org/10.1002/2017JF004373

Received 23 MAY 2017
Accepted 13 OCT 2017
Accepted article online 17 OCT 2017
Published online 26 NOV 2017

Abstract We investigate correlations between seismically derived estimates of basal acoustic impedance and basal slipperiness values obtained from a surface-to-bed inversion using a Stokes ice flow model. Using high-resolution measurements along several seismic profiles on Pine Island Glacier (PIG), we find no significant correlation at kilometer scale between acoustic impedance and either retrieved basal slipperiness or basal drag. However, there is a stronger correlation when comparing average values along the individual profiles. We hypothesize that the correlation appears at the length scales over which basal variations are important to large-scale ice sheet flow. Although the seismic technique is sensitive to the material properties of the bed, at present there is no clear way of incorporating high-resolution seismic measurements of bed properties on ice streams into ice flow models. We conclude that more theoretical work needs to be done before constraints on mechanical conditions at the ice-bed interface from acoustic impedance measurements can be of direct use to ice sheet models.

1. Introduction

Understanding and quantifying mechanical conditions at the interface between the ice and its underlying substrate is of key importance to the projective modeling of large ice masses. In particular, models require a description of the relationship between sliding velocity and basal stress, characterizing the bed's resistance to flow. Currently, most large-scale ice flow models use parameterized relations to describe basal sliding, which directly relate basal traction and basal sliding velocity. Constraining the possible functional relationship between these two parameters has been a long-standing research priority in glaciology, but rather little progress has been made. The most common approach to this problem is to use a sliding law motivated/justified by general theoretical arguments about basal processes (e.g., Fowler, 1986; Lliboutry, 1968; MacAyeal, 1989; Schoof, 2005; Weertman, 1957). However, such sliding laws have unknown parameters that need to be determined.

A standard method used to constrain unknown parameter values in the sliding law is model optimization. Most models use high-resolution surface observations to infer the spatial variability in basal conditions underneath the ice. This is done using formal inverse methods, originally introduced to glaciology by MacAyeal (1992, 1993). Given a model describing the ice flow, the basal conditions are derived by minimizing the misfit between the model output and real observations. These kind of model inversions have become standard procedure within glaciology over the past 25 years. The pioneering studies used simple two-dimensional ice flow models together with control methods to invert for basal stresses or sliding coefficients under ice streams (e.g., Joughin et al., 2004; MacAyeal, 1992; Vieli & Payne, 2003). More recent work extends application of inverse methods to much larger areas of an ice sheet (e.g., Pollard & DeConto, 2012; Sergienko et al., 2008). Developments have also been made using more sophisticated methods (e.g., Arthern, 2015; Arthern and Gudmundsson, 2010; Goldberg & Heimbach, 2013; Gillet-Chaulet et al., 2016; Larour et al., 2005; Raymond & Gudmundsson, 2009; Raymond Pralong & Gudmundsson, 2011; Thorsteinsson et al., 2003), sometimes together with higher-order ice flow models (e.g., Goldberg & Sergienko, 2011; Morlighem et al., 2010, 2013; Petra et al., 2012; Sergienko & Hindmarsh, 2013). These are beneficial both in terms of speed and accuracy of the solutions.

Rather than relying solely on inversion methods to determine parameter values for the basal boundary condition, an alternative approach is to learn about the basal boundary by estimating mechanical basal conditions independently of any ice flow model. One such method, advocated in a number of studies, uses seismic

measurements of acoustic properties; these measurements help infer the relative strength of the material at a glacier bed. A common approach provides values of acoustic impedance, which is the product of compressional wave velocity and density (e.g., Anandakrishnan, 2003; Anandakrishnan et al., 1998; Atre & Bentley, 1993; Smith, 1997, 2007; Smith et al., 2013). Results from these studies are based on the clear assumption that acoustic impedance values provide insight into the mechanical state of the subglacial material, distinguishing between different bed types, such as dilated and deforming sediments. Active source seismic surveys on Rutford Ice Stream, for example, have shown that the ice stream is underlain by soft, water-saturated sediments, with a clear boundary between high porosity deforming sediments and lower porosity sediments where the ice slides over the bed (Smith, 1997; Smith & Murray, 2009). Furthermore, passive seismic surveys have shown that locations of higher-friction "sticky spots" coincide with regions of lower porosity sediments at the bed (Smith et al., 2015). Such results therefore suggest there is potential for these approaches to provide constraints on the form of the sliding law and values of its parameters for ice flow modeling. This has indeed been part of the motivation for some recent seismic surveys (e.g., Brisbourne et al., 2017), which were combined with high-resolution radar and topography surveys.

Nevertheless, despite both optimization and seismic approaches currently being taken, little work has been done in incorporating results from seismic surveys into estimates of basal stress. In this study, we therefore investigate how results from seismic surveys can be used to further constrain the basal shear stress inferred from inverse methods. The only previous work that considers this is Vaughan et al. (2003). That study considered the correlations between mean acoustic impedance and both mean basal shear stress and slipperiness across four Antarctic ice streams; they concluded that acoustic impedance correlated well with both, and particularly slipperiness. Their work used a number of crude simplifying assumptions. For example, mean basal stress was calculated using a stress balance applied across the entire width of the ice stream, assuming the driving stress acts uniformly across it. They then balanced the driving stress with mean basal shear stress and an estimate of the mean lateral shear from the margins. This simple calculation cannot be expected to hold at a local scale with nonlocal stresses incorporated. We therefore investigate whether this result applies at higher model resolutions over which ice flow behavior has to be resolved in current ice sheet models.

As part of the iSTAR project, high-resolution bed and surface elevation data were collected over six 15×10 km^2 areas of PIG. Using an advanced 3-D Stokes model, we derive the basal conditions that minimize the misfit between modeled and observed surface velocity fields over these iSTAR sites. A clear benefit of having such high-resolution bed elevation data is that we can expect results of the inverse method to resolve genuine variations in basal properties where they have an effect on the pattern of ice flow; applying an inverse method over an area with a lower resolution map of the bed might produces some synthetic basal drag patterns that are in fact due to unresolved bed features. This is the reason we only consider these high-resolution sites in this study, so not to confuse the two issues. A separate paper will address the separation of form drag from skin drag. Over these same areas seismic reflection profiles were acquired (Brisbourne et al., 2017). We compare our high-resolution inversion results with estimates of acoustic impedance derived from the completely independent seismic profiles. Specifically, we look directly at the correlations over each of the iSTAR data sites.

The paper is structured as follows. In section 2 we present the data sets and describe the numerical model used to invert for basal traction and slipperiness. In section 3 we present the results, before carrying out analysis and comparisons with the seismic results in section 4. Finally, we make some concluding remarks in section 5.

2. Data and Model

2.1. Data

We use newly acquired, high-resolution bed and surface measurements from iSTAR field work for this study. Bed geometry was derived from ground-based radar surveys conducted over six 10×15 km^2 grids on PIG tributaries; DELORES (Deep-Looking Radio Echo Sounder) radar (King et al., 2016) was used over each site to acquire twenty two 15 km radar profiles orthogonal to the ice flow, with a 0.5 km spacing between profiles. This resulted in the first subkilometer-scale basal topography data set across tributaries of PIG. Further details about the data sets and their acquisition can be found in Bingham et al. (2017). For reference, Figure 1 shows these bed elevation data, alongside the surface elevation and surface velocity data (Landsat8 velocities, Fahnestock et al., 2016) for five of these areas. They are precisely the patches used for the modeling part

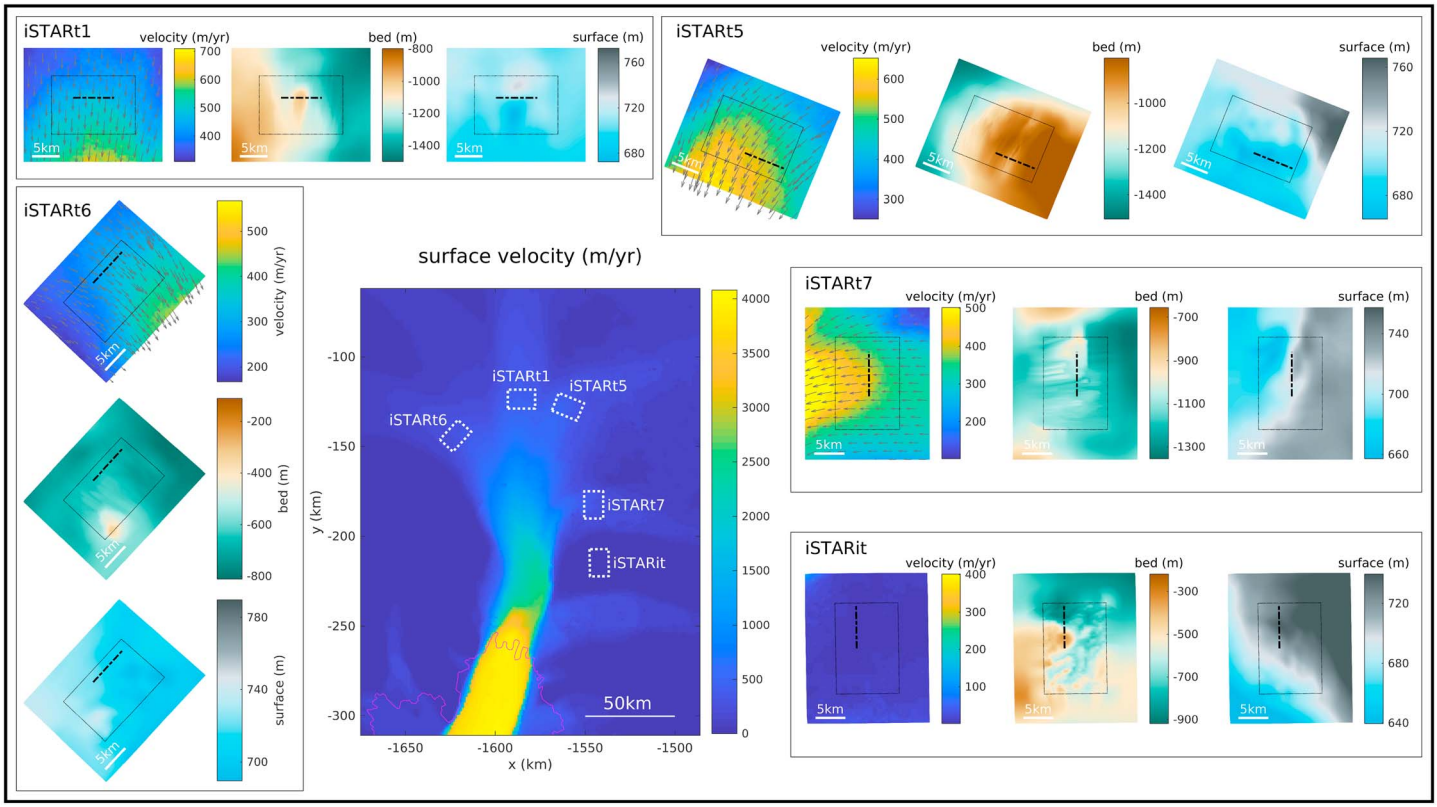

Figure 1. Location of high-resolution data patches on Pine Island Glacier that are used in this study. For each of the locations we show the velocity (Fahnestock et al., 2016), together with the bed and surface elevation fields (plotted relative to sea level). The thin black dashed box outlines the 10×15 km^2 area over which the DELORES elevation data were collected; the data are merged with BEDMAP2 elevations outside of this box (Fretwell et al., 2013). The thick black dashed line shows the location of the seismic profiles from Brisbourne et al. (2017), and the pink line on the main plot is the grounding line.

of the work. Specifically, the area covered by DELORES is extended by 5 km in each direction to avoid boundary effects influencing results over the high-resolution data area. This is done by merging the DELORES data into BEDMAP2 (Fretwell et al., 2013), smoothing over a 3 km distance from the outer edge of the DELORES patch.

Furthermore, over each of these tributary sites, a 7 km cross-stream seismic reflection profile was also acquired and analyzed (Brisbourne et al., 2017). The exact location of each of these is illustrated by the black dashed line across each patch in Figure 1. Along each profile measurements were made of acoustic impedance. The data are illustrated in Figure 4, where they are plotted alongside results from the inversions over each site. The data suggest that there are relatively uniform conditions underneath these PIG tributaries, resulting from the presence of a readily deformable and mobile sediment layer. In this study, we compare these measurements of acoustic impedance with results from the inversion that is outlined in the following section.

2.2. Model

2.2.1. Forward Model

We consider the isothermal nonlinear Stokes equations:

$$\nabla \cdot \mathbf{u} = 0, \tag{1}$$

$$\nabla \cdot \sigma + \rho \mathbf{g} = \mathbf{0}, \tag{2}$$

where ρ is the ice density, $\mathbf{g} = (0, 0, -g)$ is the gravity vector, $\mathbf{u} = (u, v, w)$ is the ice velocity vector, and σ the stress tensor. The stress tensor is given by

$$\sigma(\mathbf{u}, p) = -p\mathbf{I} + \tau(\mathbf{u}), \tag{3}$$

where p is the pressure and $\boldsymbol{\tau}$ the deviatoric stress tensor. The deformation of the ice is described by the following constitutive relation:

$$\boldsymbol{\tau} = 2\eta\dot{\boldsymbol{\epsilon}}, \tag{4}$$

$$\eta = \frac{1}{2}A^{-1/n}\,\dot{\epsilon}_{II}^{(1-n)/2n}, \tag{5}$$

$$\dot{\boldsymbol{\epsilon}} = \frac{1}{2}\left(\boldsymbol{\nabla}\mathbf{u} + \boldsymbol{\nabla}\mathbf{u}^{T}\right), \tag{6}$$

$$\dot{\epsilon}_{II} = \frac{1}{2}Tr(\dot{\boldsymbol{\epsilon}}^{2}), \tag{7}$$

where η is the (highly nonlinear) viscosity of the ice, $\dot{\boldsymbol{\epsilon}}$ is the strain tensor, n is Glen's flow law exponent (commonly taken as 3, (Glen, 1955), A the rate coefficient, and Tr is used to represent the trace of a tensor.

We solve this over a domain, $\Omega \subset \boldsymbol{R}^3$. At the top surface, $\partial\Omega_S$, a stress-free boundary condition is applied:

$$\boldsymbol{\sigma}\cdot\hat{\mathbf{n}} = \mathbf{0}, \tag{8}$$

where $\hat{\mathbf{n}}$ is the unit normal. At the bottom surface, $\partial\Omega_B$, we have

$$\mathbf{T}\left(\boldsymbol{\sigma}\cdot\hat{\mathbf{n}}\right) = -C^{-1/m}|\mathbf{Tu}|^{1/m-1}\,\mathbf{Tu}, \tag{9}$$

$$\mathbf{u}\cdot\hat{\boldsymbol{n}} = 0, \tag{10}$$

where m is the sliding exponent, C the sliding coefficient (often referred to as the "slipperiness"), and $\mathbf{T} = \mathbf{I} - \hat{\mathbf{n}}\otimes\hat{\mathbf{n}}$ is the tangential projection operator. This corresponds to a Weertman-style sliding law in the tangential direction (Weertman, 1957) and a no-penetration condition in the normal direction. Furthermore, to ensure positivity of the sliding coefficient, C, we replace it by the parameterizaton $\kappa = \ln(C)$ in equation (9).

Finally, at the edges of the domain, $\partial\Omega_E$, we apply Dirichlet boundary conditions on the velocity field,

$$\mathbf{u} = \mathbf{u}_{\text{obs}}(x,y) + \mathbf{u}_{\text{corr}}(z), \tag{11}$$

where $\mathbf{u}_{\text{obs}}(x,y)$ are the surface velocities from Landsat8 (Fahnestock et al., 2016) and $\mathbf{u}_{\text{corr}}(z)$ is a small correction for depth dependance of ice velocity from vertical shearing.

2.2.2. Inverse Model Approach

Given the forward 3-D Stokes model, we seek to apply an inverse method to estimate the spatial distribution of the basal slipperiness, C (as defined through equation (9)), at the ice-bed interface. With a pattern of surface velocity data, $\mathbf{u}_{\text{obs}}$, the inverse problem involves minimizing the misfit between the velocity observations and horizontal model output surface velocities, $\mathbf{u}_H = (u, v, 0)$, to infer the slipperiness field that allows the best fit of observations to data. As in previous work (e.g., Petra et al., 2012), this is formulated as a nonlinear, least squares minimization problem of the cost functional:

$$\begin{aligned}\mathcal{J}(\mathbf{u},\kappa) &= \mathcal{J}_{\text{mis}} + \mathcal{J}_{\text{reg1}} + \mathcal{J}_{\text{reg2}} \\ &= \frac{1}{2}\int_{\partial\Omega_S}|\mathbf{u}_H - \mathbf{u}_{\text{obs}}|^2\,\mathrm{d}\mathbf{s} + \frac{1}{2\gamma^2}\int_{\partial\Omega_B}\boldsymbol{\nabla}\kappa\cdot\boldsymbol{\nabla}\kappa\mathrm{d}\mathbf{s} + \frac{1}{2\beta^2}\int\kappa\cdot\kappa\mathrm{d}V\end{aligned} \tag{12}$$

where $\kappa = \ln(C)$ and γ and β are parameters governing the relative size of the Tikhonov-style regularization terms and the misfit term. Without any regularization the problem is ill posed. The first Tikhonov term, $\mathcal{J}_{\text{reg1}}$, enforces smoothness of the control variable; this is the same approach as in many other studies (e.g., Goldberg & Heimbach, 2013; Morlighem et al., 2013; Petra et al., 2012). It defines a length scale over which we expect variations in κ to occur. This is important so as not to get variations in κ on length scales that are less than those which can be resolved given surface observations (e.g., Gudmundsson, 2003). The size of γ therefore governs the relative importance of the data misfit (from $\mathcal{J}_{\text{mis}}$) and imposing smoothness (from $\mathcal{J}_{\text{reg1}}$). $\mathcal{J}_{\text{reg2}}$ is only needed due to code implementation issues; κ has to be defined throughout the 3-D domain, and so the term acts to regularize κ toward zero away from the basal boundary. The coefficient of this term is several orders of magnitude smaller than that on $\mathcal{J}_{\text{reg1}}$ (Table 1), and it therefore does not affect behavior at the boundary.

Table 1
List of all Variables and Parameters

Parameter	Value	Units	Description
$\mathbf{u}$		myr^{-1}	Ice velocity
p		kPa	Pressure
$\boldsymbol{\sigma}$		kPa	Stress tensor
$\boldsymbol{\tau}$		kPa	Deviatoric stress tensor
$\dot{\boldsymbol{\epsilon}}$		yr^{-1}	Strain rate tensor
$\dot{\epsilon}_{II}$	$\frac{1}{2}Tr(\dot{\boldsymbol{\epsilon}}\dot{\boldsymbol{\epsilon}})$,	yr^{-1}	Symmetric strain rate
ρ	917	kgm^{-3}	Ice density
g	9.81	ms^{-2}	Gravitational acceleration
η	$\frac{1}{2}A^{-1/n}\ \dot{\epsilon}_{II}^{(1-n)/2n}$	kPa yr	Ice viscosity
A	$A(T)$	$\mathrm{kPa}^{-n}\mathrm{yr}^{-1}$	Rate coefficient in Glen's law
n	3		Exponent in Glen's law
$\boldsymbol{\tau}_b$		kPa	Basal stress
m	3		Exponent in Weertman sliding law
$C = \exp(\kappa)$		$\mathrm{myr}^{-1}\mathrm{kPa}^{-m}$	Sliding coefficient in Weertman sliding law
β	10^3		Coefficient of volume regularization term in (12)
γ	10^{-3}		Coefficient of Tikhonov surface regularization in (12)

2.2.3. Numerical Solution

The forward problem is written in weak form and solved using the open-source finite element computational software library, known as FEniCS (Alnæs et al., 2015; Logg et al., 2012). FEniCS provides tools for the automated solution of differential equations using finite element methods. Its environment supports automated parallelization and also uses symbolic automated differentation. The user simply defines the problem in weak form, chooses from the large library of finite elements available, and defines which numerical solvers to use. In our case, we use the Taylor-Hood P2-P1 element for velocity and pressure, respectively, (Taylor & Hood, 1973) and solve the Stokes equations using a Newton-based nonlinear solver, which is part of the PETSc package (Balay et al., 2016a, 2016b, 1997) interfaced with FEniCS. An example of a solution domain at 500 m resolution (as used for most numerical solutions presented in this paper) is given in Figure 2. To prevent blowup as either $|\dot{\boldsymbol{\epsilon}}|$ or $|\mathbf{Tu}|$ tend toward zero, a small correction parameter is added to both (7) and (9). Finally, the no-penetration condition on the bottom boundary of the domain (10) is imposed using Lagrange multipliers.

To carry out the inversion, we use capabilities in the dolfin-adjoint interface to FEniCS (Farrell et al., 2013). Using automatic differentiation, we are able to derive the full adjoint and tangent linear models. With the interfacing to optimization algorithms also built in, we are then able to use gradient descent algorithms

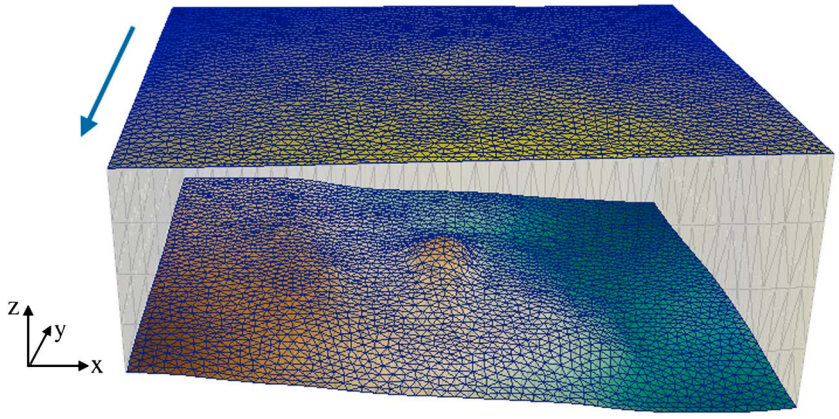

Figure 2. An example of the 20×25 km^2 solution domain for iSTARt1 at 500 m resolution (the resolution used for most simulations in this paper). Observed surface velocities are illustrated on the top of the domain, and an arrow illustrating the ice flow direction is shown. The mesh is outlined in blue.

to carry out the minimization of the cost function. Specifically, we use the limited-memory, variable-metric method, which builds an approximation to the Hessian via gradient evaluations.

We decide on the correct amount of regularization to implement by undertaking an L curve analysis; smoothness is imposed on the solution without compromising on misfit. The results from this analysis for the iSTARt1 site are shown in Appendix A. Based on the method, we choose to take $\gamma = 0.001$, since imposing less regularization than this (i.e., larger γ) does not allow for much further improvement on fitting the surface observations.

3. Estimates of Basal Properties From Model Inversion

3.1. Description of Results

We run the inverse model over the each of the $20 \times 25 \text{km}^2$ areas encompassing the five high-resolution iSTAR sites illustrated in Figure 1. These areas are each extruded vertically to give a 3-D domain. Parameter values are listed in Table 1. Results from the inverse method applied over each site are shown in Figure 3. Specifically, we show the velocity and basal elevation data for each site (Figure 3, left column), the slipperiness, we show the velocity and basal elevation data for each site, before plotting the slipperiness (Figure 3, middle column) and basal stress (Figure 3, right column). The black dashed line across each plot shows where the seismic profile was taken; we will compare the acoustic impedance measurements along these lines with the results of the inversions in the following section. We choose to plot the slipperiness, $C = e^{\kappa}$, on a linear scale, and the basal stress field, $\boldsymbol{\tau}_b$, on a logarithmic scale in order to pick out contrasting features. More specifically, on the linear scale the high slip (corresponding to low basal stress) areas stand out, while on a logarithmic scale, the high basal stress (corresponding to low slip) areas are most pronounced.

We consider in more detail the results for each of the tributaries, working around PIG clockwise from iSTARt6 (see Figure 1). We describe the spatial variability of the slipperiness and basal stress fields, commenting also on any correlations with bed/surface features.

First, the results of the inverse approach over iSTARt6 show that the highest slip region (corresponding to lowest basal shear stresses) is located on the downstream left of the DELORES grid, corresponding to where there are the largest accelerations in ice velocity. This location is also where basal elevation is lowest. There is a maximum in basal shear stress on the downstream right, positioned where the ice flows over the highest bed elevation.

The same pattern of behavior is evident over iSTARt1; the bed is more slippery to the downstream left, and this location corresponds with that of the lowest basal elevations. Moreover, there is a local maximum in basal shear stress at the center of the grid, where the peak bed elevation of the drumlin-like feature also lies. However, over this site there is not the same clear correspondence between the most slippy region and acceleration in flow speed.

Over iSTARt5 bed features are less pronounced (contours are more evenly spaced), but we do still see interesting basal stress and slipperiness fields result from carrying out the inversion. In particular, the highest slip region at the outflow of the domain corresponds to where there is a downstream negative gradient in bedrock, and a coincident speed up in velocity (with ice velocity reaching over 600 myr^{-1}).

The results from implementing the model inversion over iSTARt7 are particularly interesting due to the previously unresolved topography revealed by the high-resolution radar survey; there is a "cliff edge" feature where the bed elevation increases by approximately 300 m within ~1 km. While the surface velocity field does not have a dramatic response to this, the basal stress field derived from the inversion of surface data clearly reflects the presence of the cliff. Furthermore, the maximum basal shear stress overlies the highest bed elevation, demonstrating the form drag that results from extreme gradients in the bed. Downstream of the cliff, bed elevation decreases down to original values over about 5 km. In this more gently varying region we find the highest slip values, outside of the DELORES data grid, with an acceleration in flow velocity and resultant surface lowering by ~50 m (refer to Figure 1).

Finally, results for the inversion over the inter-tributary patch, iSTARit, have far less variation within them. However, there is still a correspondence between the most slippery/low basal stress regions and minima in bedrock elevation.

Note also that for all the sites the misfit to velocity observations at the point we terminate the inversion are small (a maximum of ~10% of the observed surface velocities). The misfit also has no visible pattern

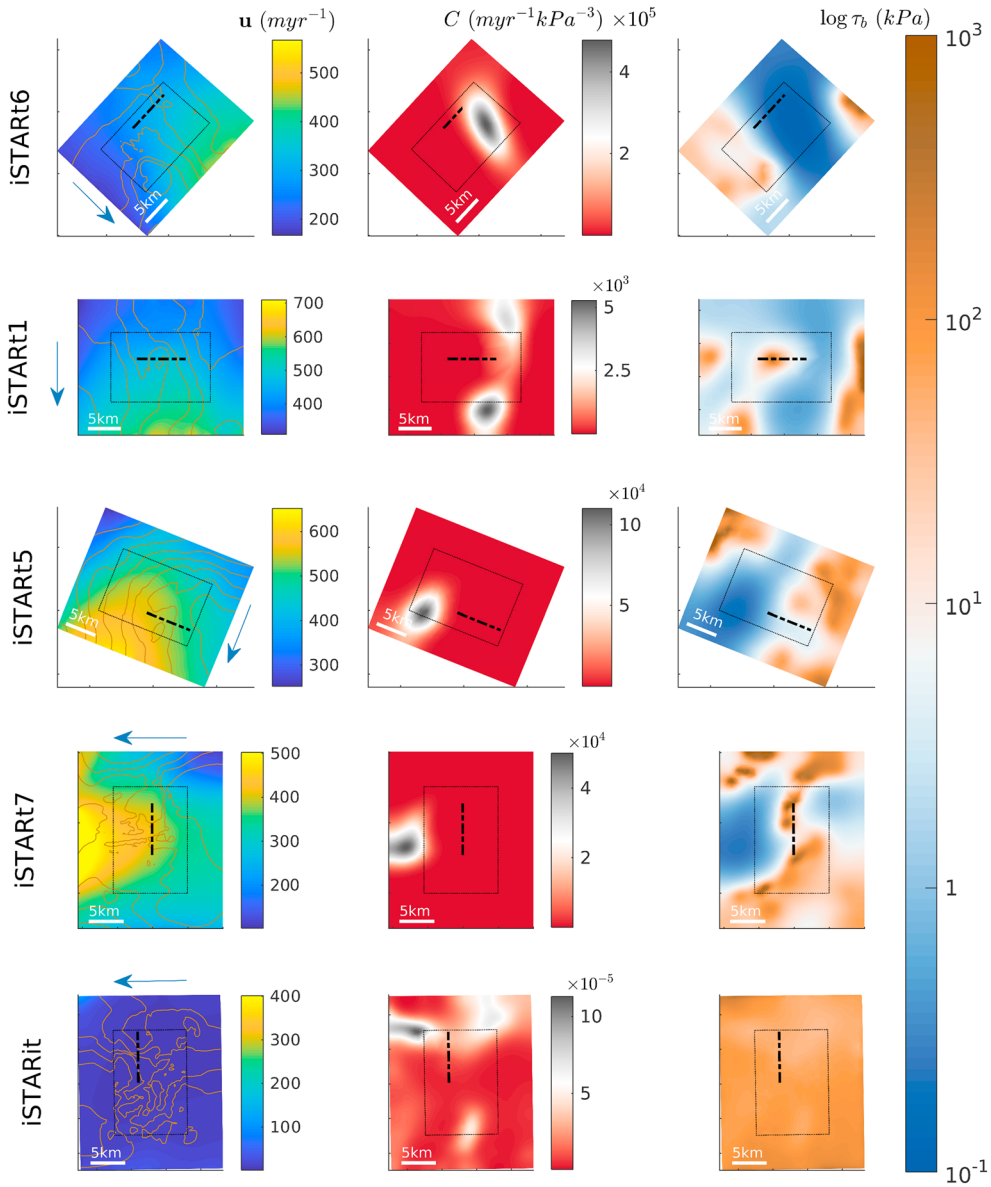

Figure 3. Results for each of the iSTAR sites.(left column) The surface velocity at each site (with an arrow showing the flow direction); the contours illustrate the elevation of the underlying bedrock (as illustrated in Figure 1) and are spaced at 100 m intervals. Alongside there is a plot showing (middle column) the inverted slipperiness field and (right column) the corresponding basal stress field. The slipperiness fields are plotted on individual color scales, as the range in values is large, while the basal stress is plotted on a log scale unified across all sites. The sites are exactly those shown in Figure 1, starting at iSTARt6 and moving clockwise around the tributaries.

or structure away from the boundary of the extended domain where the Dirichlet boundary conditions are implemented.

3.2. Parameter Study

A set of tests have shown that both the high and low slipperiness regions identified are consistent across a range of parameter choices. These include parameters in the ice flow model (e.g., sliding law exponent (9)), parameters for the numerical solution (e.g., resolution and the initial slipperiness guess that starts the optimization) and parameters in the inversion (e.g., β and γ (12)).

Considering different values of other parameters in the sliding law, specifically m is important as this can be seen as a way of representing different physical processes occurring at the bed. The Weertman sliding law we have used in this work was originally derived to describe the slip of ice over a hard bed (Weertman, 1957).

The value of m corresponds to the creep exponent in Glen's flow law describing the rheology of the ice. Until now, it has therefore been taken as 3. However, others have shown that by varying the exponent in the sliding law, different processes can be represented, including those that are perhaps more likely to be occurring at the bed of PIG. In particular, taking $m = 1$ mimics viscous deformation of the till (MacAyeal, 1989; Hindmarsh, 1997) and letting $m \to \infty$ results in purely plastic behavior (e.g., Joughin et al., 2004; Tulaczyk et al., 2000; Tulaczyk, 2006). We therefore chose to run a suite a simulations with varying values of m and saw consistency in the pattern of results across a whole range.

Furthermore, the inverse problem is ill posed and it is therefore important to consider a range of solutions. First, the optimization problem may permit local minimizers (since it is nonconvex); we therefore solve the inversion starting the optimization algorithm from several different initial guesses. Regardless of initial guess, solutions agree on the slipperiness field. This increases our confidence that the inversion has in fact found a global minimum rather than one of many possible local minima. Second, we also consider the range of solutions that result from varying the relative size of terms in the cost function (12). The location of highs and lows in basal slipperiness remains consistent.

4. Analysis and Discussion

4.1. Comparison of Results With Estimates of Basal Properties From Seismic Surveys

The main objective of this study was to compare basal properties estimated by model inversion with derived values of acoustic impedance for the material underlying the ice. In this section we therefore consider the inferred basal stress and slipperiness fields in the locations where Brisbourne et al. (2017) undertook seismic lines and have derived the corresponding acoustic impedance measurements. Figure 4 is a plot of these slipperiness and basal shear stress fields (from the numerical solutions shown in Figure 3) together with the acoustic impedance along the seismic lines at each site (Brisbourne et al., 2017). The Spearman's rank correlation coefficients between the acoustic impedance and $\kappa = \ln(C)$, $\left(r_{A\kappa}\right)$, and between the acoustic impedance and $\log \tau_b$, $\left(r_{AT}\right)$, are also included on each of the plots, informing us of how well the relationship between each pair of variables can be described by a monotonic function.

We consider each of the profiles in detail. Along the iSTARt6 profile, the slipperiness increases to left of flow (toward the most slippy region evident in Figure 3). The basal stress correspondingly decreases. Neither field, however, picks up the local variation seen in the acoustic impedance measurements, and correlation between the fields is weak, with magnitude $|r| \approx 0.2$.

Over iSTARt1 the local maximum in basal stress lies ~22 km along the seismic line. This corresponds to where both the bed elevation and acoustic impedance are also at maximum values. Furthermore, there is more variation in the acoustic impedance values in this central profile section overlying the region with higher basal stress values. The correlations between the acoustic impedance and the slipperiness/basal shear stress are higher here ($|r| \approx 0.39$) at a significance level of ≈10%.

On iSTARt5 there seems to be a clear divide visible in the acoustic impedance measurements; along the first 4 km of the profile there is a great deal of local variation before the measurements become much smoother over the second half of the profile. The second section of the line is where the inferred basal shear stress reaches higher values, though still low compared to over the central section of iSTARt1. The relationship between acoustic impedance and the slipperiness/basal shear stress is stronger.

The profile over iSTARt7 has the lowest correlation between acoustic impedance measurements and the estimated basal stress field of all the sites, $|r| \approx 0.1$. There is also slightly more spatial variation in basal stress and slipperiness than there is along the other seismic lines. We expect that this is largely down to the seismic profile overlying part of the significant feature in the bed (see Figure 1). The high slip/low basal stress ~2–3 km along the line corresponds with where there is a rapid change in bed elevation. Furthermore, along the half of the seismic profile that overlies the elevated bed, acoustic impedance varies less.

Finally, over iSTARit the correlation is somewhat more significant, particularly between the slipperiness and acoustic impedance, $r_{A\kappa} \approx -0.6$. The acoustic impedance shows little variation apart from between ~3.5 and 5.5 km in the central section of the profile; this location corresponds with where there is steep topography. The slipperiness (and basal shear stress) are also relatively constant at either end of the seismic line, just fluctuating over the same central section where the acoustic impedance varies. We hypothesize that this

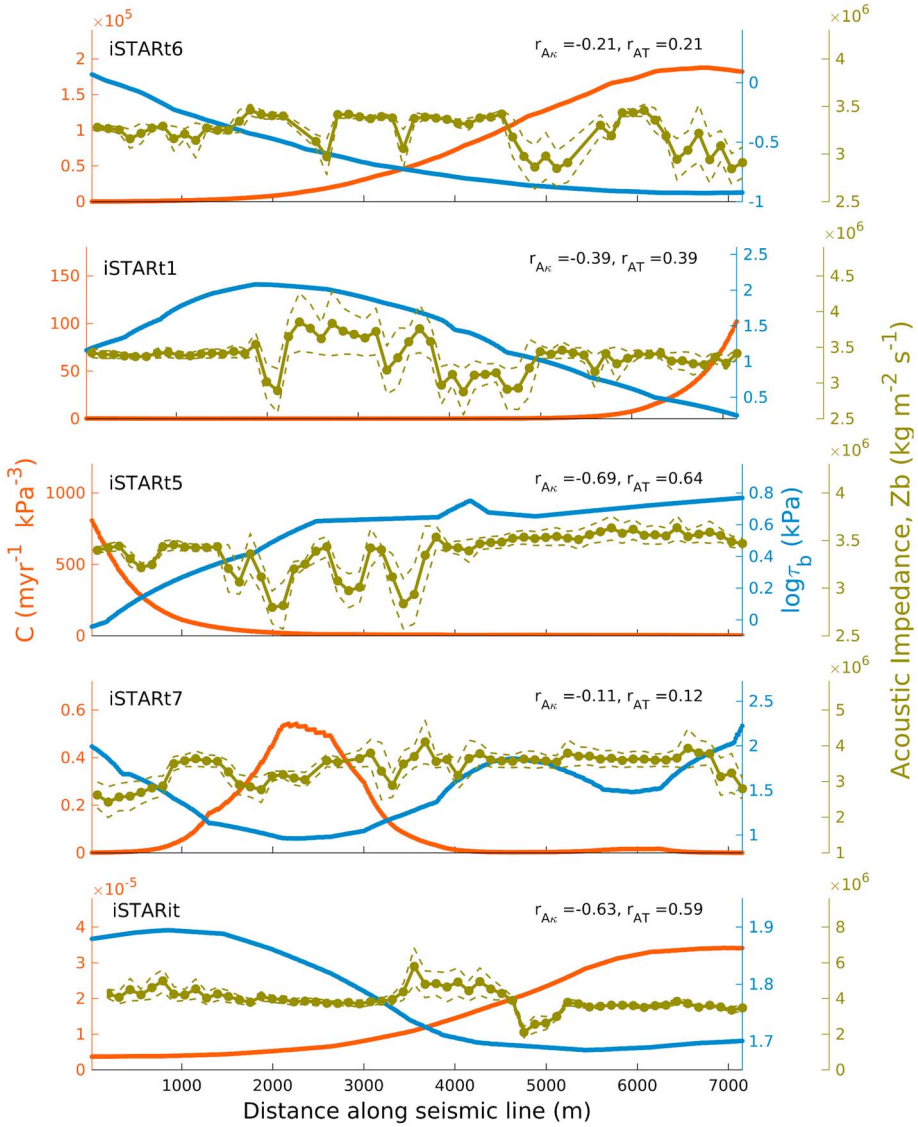

Figure 4. Values of the basal slipperiness C (red), the basal shear stress τ_b (blue), and acoustic impedance (green dots) along the seismic line for each iSTAR site. Slipperiness and basal stress are calculated from the inversion described in section 3, and acoustic impedances come from Brisbourne et al. (2017). The location of each seismic profile is illustrated by the dotted line across each patch in Figure 3. The Spearman's correlation coefficients between the acoustic impedance and logarithm of the slipperiness $(r_{A\kappa})$ and between the acoustic impedance and the logarithm of the basal stress (r_{AT}) are stated in the top right hand corner of each plot.

higher correlation could be related to the fact that this is the one transect where the basal till is likely not deforming strongly.

Overall, the most noticeable feature of the set of profiles is that the slipperiness and basal stress fields do not vary on a length scale as small as that which the acoustic impedance varies over. Given that we had used the L curve analysis to choose regularization resulting in the smoothest possible solution that minimizes the misfit between modeled and surface velocities, we also consider the possibility that in reality, the basal conditions are not as smooth. In the supporting information, we include a figure (Figure S1) where solutions have been found when less regularization is imposed on the inversion, taking $\gamma = 0.01$. This corresponds to decreasing the ratio between the regularization and misfit terms in the cost function (see equation (12)) by a factor of 100. While this does introduce slightly more spatial variability, the correlations between fields are worse, not better. Furthermore, the variability in magnitude of the solutions grows considerably. The regularization therefore appears to play a stronger role in suppressing magnitude variation than in limiting the length scale

of variations. This suggests that were we to decrease the regularization further so that the spatial variability of the slipperiness solutions matched that of the acoustic impedance measurements, the variation in magnitude would become unreasonably large.

Finally, in the supporting information we also include a plot of solutions over site iSTARt7 for varying values of the exponent in the sliding law, m (see Figure S2). The reasoning for this was discussed in section 3.2. Moreover, we choose to illustrate this parameter test over iSTARt7 since the correlations here were lowest with $m = 3$. First we considered results with $m = 1$ to mimic Vaughan et al. (2003) who assumed a linear sliding law. Furthermore, Brisbourne et al. (2017) suggested that the tributaries are underlain by deformable sediments (though this is not to say that the sediments are certainly deforming viscously, as represented through taking $m = 1$). In contrast, Gillet-Chaulet et al. (2016) suggested that observed surface velocity accelerations on PIG are best reproduced using a sliding law with $m \geq 5$. We therefore also plot results with two larger values of m (= 5, 10) to see if a more plastic description of the till allows for better fit. However, there are only very slight improvements in the correlations between results of the inversion and measurements of acoustic impedance. This is a consistent result across all sites; correlations remain consistently low regardless of the value of m.

4.2. Correlation on a Large Scale

In the previous section we considered the correlation between individual measurements of acoustic impedance and results of an inversion and found very limited correlation. We now consider the possibility that although no significant correlation is found within each seismic profile, there may be correlation between average profile values. While large-scale variation in basal slipperiness can be detected without the need for any measurements of the bed (i.e., from surface slopes and surface velocities), it would be reassuring to confirm that bed properties estimated by seismic methods agree with those estimates from inversion methods at the larger scales.

To do this, we took the mean acoustic impedance along each 7 km profile and plot it against (a) the mean basal slipperiness along the profile and (b) the mean basal stress along the profile. These mean values for each site are labeled in the two plots in Figure 5, and the Spearman's rank correlation coefficients between acoustic impedance and $\kappa = \ln(C)$ (coefficient denoted by $r_{A\kappa}$) and between acoustic impedance and the logarithm of basal shear stress (r_{AT}) are shown in the legend for both plots. Note that as well as plotting the mean values along each complete seismic profile, we also split each profile in two and calculate the corresponding mean values (illustrated by the medium-sized dots) and then split each domain into four and calculate the corresponding mean values once again (illustrated by the smallest-sized dots). The correlation coefficients between points across each of these length scales are also shown in the legend.

Comparing the two plots in Figure 5, we observe monotonic relationships between variables. Since these do not appear to be linear, we consider the more general Spearman's rank correlation coefficient. This coefficient assesses how well the relationship between mean basal slipperiness/shear stress and mean acoustic impedance can be described by a monotonic function. Values are included in the legend of the plots in Figure 5. We perform a simple hypothesis test for the significance of the correlation coefficients and find the correlations to be significant at the 13% level when considering the five averaged profile values (largest dots on plots). Furthermore, despite the values of $r_{A\kappa}$ and r_{AT} decreasing in magnitude, they are more statistically significant (at the 4% and 0.05% levels, respectively) when averaging over the shorter length scales within each profile. Considering these averages across different profiles has introduced enough variation to make us confident of some significance to the correlation between estimates of basal ice mechanics from inverse methods and measured acoustic impedance values over long enough length scales.

It is also worth remarking on the fact that the Pearson's correlation coefficient for between-profile linear correlation is stronger between the slipperiness and acoustic impedance $\left(r^p_{A\kappa} = -0.84\right)$ than it is between the basal shear stress and acoustic impedance $\left(r^p_{AT} = 0.67\right)$. This is in agreement with Vaughan et al. (2003) who saw correlations of 0.8 and 0.6, respectively, when looking at values averaged over entire ice streams.

Finally, it is important to point out that no detailed functional theory currently exists relating the slipperiness/basal stress fields to acoustic impedance of the sediment. Acoustic impedance depends on several properties of the bed, including effective pressure, many of which link directly back to the sliding law. If a physical theory were developed, we would also expect there to be other unknown parameters in the relationship, such as grain size of the sediment, which would require measurements. As an alternative, if we took a function that fitted the data in Figure 5 as an estimate of a relationship, it would be an interesting experiment

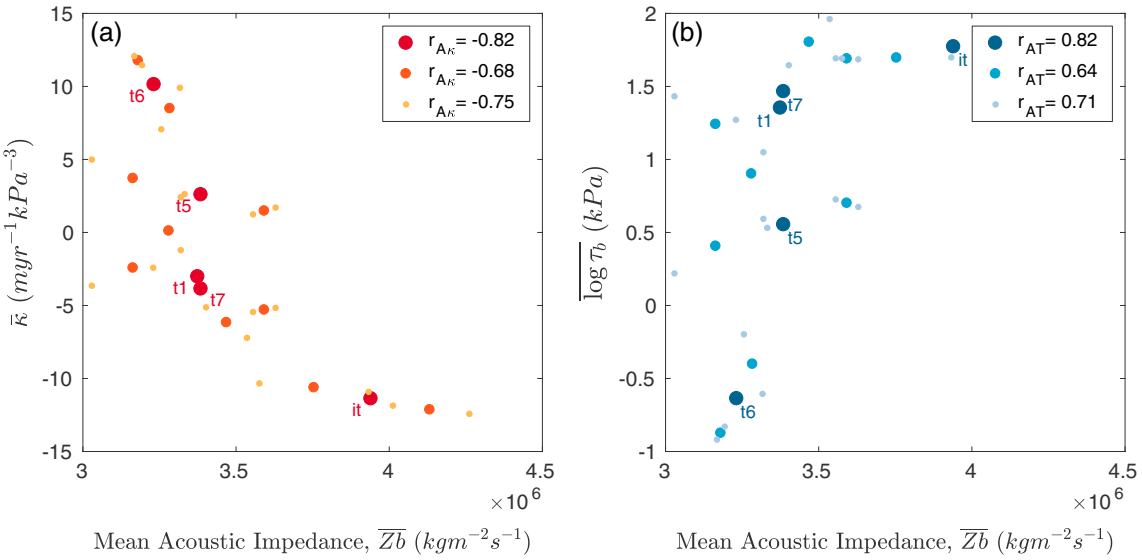

Figure 5. The mean acoustic impedance from each of the seismic profiles plotted against mean values of (a) $\kappa = \ln(C)$ and (b) $\log \tau_b$. In both the largest dots show the mean values taken across each 7 km profile (as labeled); the medium dots are the mean values taken over each half of each domain; the smallest dots are the mean values taken over each quarter of each domain. The Spearman correlation coefficients between the points averaged over each distance are stated in the legend.

to see what solution the forward model produced with C varying on this same length scale that the acoustic impedance varies on. Would this further reduce the surface velocity misfit? However, given that this would require a full 2-D grid of acoustic impedance measurements, this is something we cannot carry out here given the available data. Instead, we suggest that in the future further thought should be put into locations of any seismic surveys that are to be carried out. It would be useful to place seismic lines in 2-D grids over the relevant spatial scales, and in locations where results from inverse methods do suggest meaningful changes in basal properties.

5. Conclusions

In this study we have used newly acquired, high-resolution bed and surface elevation data to carry out inversions for basal slipperiness underneath PIG using a full Stokes ice flow model. We have made comparisons with seismically derived estimates of acoustic impedance over the same areas. There is no consistent correlation between the slipperiness and acoustic impedance within each seismic profile, but a stronger correlation is present when averaging values over ice thickness length scales and comparing these average values across distinct profiles. This is expected given that both acoustic impedance values and ice surface characteristics are a direct consequence of the basal conditions of the ice sheet; it makes sense that there is some correlation between the methods of quantifying basal conditions.

We consider the lack of correlation at the shorter scale that acoustic impedance varies over. We hypothesize these variations are not at a length scale that is of importance to the large-scale ice sheet flow, since inverting with high-resolution surface observations does not reproduce variations in basal conditions on this scale. This is also consistent with more theoretical studies (e.g., Gudmundsson, 2003) that consider the length scales of basal variability that one would expect to be represented on the surface. It therefore seems logical that over the long scales, which do affect ice dynamics, there is correlation between results from modeling and seismic approaches, whereas over the shorter length scales, there is not.

An objective of this study was to compare and contrast two research approaches to quantifying bed strength underneath the ice. While the modeling community recognizes the strong role played by the bed, and the need, if possible, to recover as detailed a representation of this bed strength as possible, they have as yet not been able to constrain estimates from modeling approaches with observations. There is no question that seismic exploration is capable of discriminating variability in basal conditions (e.g., Luthra, 2017; Smith & Murray, 2009); however, results from such exploration cannot currently be used as quantitative input for ice sheet models. Only with a physical theory relating acoustic impedance to either basal shear stress

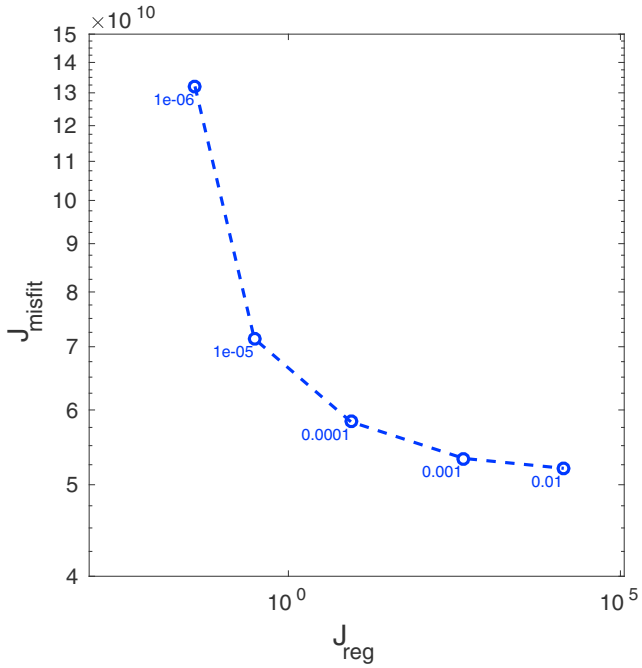

Figure A1. The L curve: a log-log plot of the misfit term, J_{misfit}, against the regularization term, J_{reg} in (12). Each point is labeled with a value of γ, where γ^2 is the ratio of the coefficient of the misfit term to the regularization term.

or a parameter in a physical sliding law would we be able to start to consider the potential for acoustic impedance measurements to be used as an a priori constraint on the mechanical conditions at the ice-bed interface in ice flow models. While results from this study do suggest that there is the potential for seismic studies to be useful to ice sheet modeling in the future, such theoretical progress certainly needs made first. Further seismic coverage that may be useful for this would have to be 2-D and well placed, spanning significant changes in bed conditions.

Appendix A: L Curve Analysis

We plot the magnitude of the misfit and regularization terms in (12) for a range of values of γ in Figure A1. It is clear that decreasing regularization (i.e., increasing γ) beyond a certain level has limited impact on how small the misfit term becomes. Based on this curve, we choose to use $\gamma = 0.001$ in the inverse problem described in this paper.

Acknowledgments
We would like to thank Alex Brisbourne and Andy Smith for useful discussions and providing data, David Vaughan and Rob Arthern for useful discussions and feedback on a first draft, and Rob Bingham for giving us access to the radar data in advance of publication. We would also like to thank Olaf Eisen, Huw Horgan, and Daniel Goldberg for extremely useful reviews, which helped to improve the manuscript significantly. This work was supported by funding from the UK Natural Environment Research Council's iSTAR Programme and NERC grant NE/J005754/1. Farrell is supported by EPSRC grant EP/K030930/1. Data are available from the iStar GIS (http://gis.istar.ac.uk) and from the NERC Polar Data Centre.

References

Alnæs, M. S., Blechta, J., Hake, J., Johansson, A., Kehlet, B., Logg, A., … Wells, G. N. (2015). The FEniCS project version 1.5. *Archive of Numerical Software*, *3*(100), 9–23. https://doi.org/10.11588/ans.2015.100.20553

Anandakrishnan, S. (2003). Dilatant till later near the onset of streaming flow of Ice Stream C, West Antarctica, determined by AVO (amplitude vs offset) analysis. *Annals of Glaciology*, *36*(1), 283–286. https://doi.org/10.3189/172756403781816329

Anandakrishnan, S., Blankenship, D. D., Alley, R. B., & Stoffa, P. (1998). Influence of subglacial geology on the position of a West Antarctic ice stream from seismic observations. *Nature*, *394*(1), 62–65. https://doi.org/10.1038/27889

Arthern. R. J. (2015). Exploring the use of transformation group priors and the method of maximum relative entropy for Bayesian glaciological inversions. *Journal of Glaciology*, *61*(229), 947–962. https://doi.org/10.3189/2015JoG15J050

Arthern, R. J., & Gudmundsson, G. H. (2010). Initialization of ice-sheet forecasts viewed as an inverse Robin problem. *Journal of Glaciology*, *56*(197), 527–533. https://doi.org/10.3189/002214310792447699

Atre, S., & Bentley, C. (1993). Laterally varying basal conditions beneath Ice Streams B and C, West Antarctica. *Journal of Glaciology*, *39*(133), 507–514. https://doi.org/10.1017/S0022143000016403

Balay, S., Gropp, W. D., McInnes, L. C., & Smith, B. F. (1997). Efficient management of parallelism in object oriented numerical software libraries. In E. Arge, A. M. Bruaset, & H. P. Langtangen (Eds.), *Modern Software Tools in Scientific Computing* (pp. 163–202). Birkhäuser Press.

Balay, S., Abhyankar, S., Adams, M. F., Brown, J., Brune, P., Buschelman, K., … Zhang, H. (2016a). PETSc Web page. Retrieved from https://www.mcs.anl.gov/petsc

Balay, S., Abhyankar, S., Adams, M. F., Brown, J., Brune, P., Buschelman, K., … Zhang, H. (2016b). PETSc users manual (Tech. Rep., ANL-95/11 - Revision 3.7). Argonne National Laboratory.

Bingham, R. G., Vaughan, D. G., King, E. C., Davies, D., Cornford, S. L., Smith, A. M., … Shean, D. E. (2017). Diverse landscapes beneath Pine Island Glacier influence ice flow. *Nature Communications*. https://doi.org/10.1038/s41467-017-01597-y

Brisbourne, A. M., Smith, A. M., Vaughan, D. G., King, E. C., Davies, D., Bingham, R. G., … Rosier, S. H. R. (2017). Bed conditions of Pine Island Glacier, West Antarctica. *Journal of Geophysical Research: Earth Surface*, *122*, 419–433. https://doi.org/10.1002/2016JF004033

Fahnestock, M., Scambos, T., Moon, T., Gardner, A., Haran, T., & Klinger, M. (2016). Rapid large-area mapping of ice flow using Landsat 8. *Remote Sensing of Environment*, *185*, 84–94. https://doi.org/10.1016/j.rse.2015.11.023

Farrell, P. E., Ham, D. A., Funke, S. W., & Roges, M. E. (2013). Automated derivation of the adjoint of high-level transient finite element programs. *SIAM Journal on Scientific Computing*, *35*(4), C369–C393. https://doi.org/10.1137/120873558

Fretwell, P., Pritchard, H. D., Vaughan, D. G., Bamber, J. L., Barrand, N. E., Bell, R., … Zirizzotti, A. (2013). Bedmap2: Improved ice bed, surface and thickness datasets for Antarctica. *The Cryosphere*, *7*, 375–393. https://doi.org/10.5194/tc-7-375-2013

Fowler, A. C. (1986). A sliding law for glaciers of constant viscosity in the presence of subglacial cavitation. *Proceedings of the Royal Society A*, *407*(1832), 147–170. https://doi.org/10.1098/rspa.1986.0090

Gillet-Chaulet, F., Durand, G., Gagliardini, O., Mosbeux, C., Mouginot, J., Rémy, F., & Ritz, C. (2016). Assimilation of surface velocities acquired between 1996 and 2010 to constrain the form of the basal friction law under Pine Island Glacier. *Geophysical Research Letters*, *43*, 10,311–10,321. https://doi.org/10.1002/2016GL069937

Glen, J. W. (1955). The creep of polycrystalline ice. *Proceedings of the Royal Society A*, *228*(1175), 519–538. https://doi.org/101098/rspa.1955.0066

Goldberg, D. N., & Heimbach, P. (2013). Parameter and state estimation with a time-dependent adjoint marine ice sheet model. *The Cryosphere*, *7*(6), 1659–1678. https://doi.org/10.5194/tc-7-1659-2013

Goldberg, D. N., & Sergienko, O. V. (2011). Data assimilation using a hybrid ice flow model. *The Cryosphere*, *5*, 315–327. https://doi.org/10.5194/tc-5-315-2011

Gudmundsson, G. H. (2003). Transmission of basal variability to a glacier surface. *Journal of Geophysical Research*, *108*(B5), 2253. https://doi.org/10.1029/2002JB002107

Hindmarsh, R. C. A. (1997). Deforming beds: Viscous and plastic scales of deformation. *Quaternary Science Reviews*, *16*, 1039–1056. https://doi.org/10.1016/S0277-3791(97)00035-8

Joughin, I., MacAyeal, D. R., & Tulaczyk, S. (2004). Basal shear stress of the Ross ice streams from control method inversions. *Journal of Geophysical Research*, *109*, B09405. https://doi.org/10.1029/2003JB002960

King, E. C., Pritchard, H. D., & Smith, A. M. (2016). Subglacial landforms beneath Rutford Ice Stream, Antarctica: Detailed bed topography from ice-penetrating radar. *Earth System Science Data*, *8*(1), 151–158. https://doi.org/10.5194/essd-8-151-2016

Larour, E., Rignot, E., Joughin, I., & Aubry, D. (2005). Rheology of the Ronne Ice Shelf, Antarctica, inferred from satellite radar interferometry data using an inverse control method. *Geophysical Research Letters*, *32*, l05503. https://doi.org/10.1029/2005GL021693

Lliboutry, L. (1968). General theory of subglacial cavitation and sliding of temperate glaciers. *Journal of Glaciology*, *7*(49), 21–58. https://doi.org/10.3198/1968JoG7-49-21-58

Logg, A., Mardal, K.-A., & Wells, G. N. (Eds.) (2012). *Automated solution of differential equations by the finite element method*. Berlin: Springer. https://doi.org/10.1007/978-3-642-23099-8

Luthra, T., Peters, L. E., Anandakrishnan, S., Alley, R. B., Holschuh, N., & Smith, A. M. (2017). Characteristics of the sticky spot of Kamb Ice Stream, West Antarctica. *Journal of Geophysical Research: Earth Surface*, *122*, 641–653. https://doi.org/10.1002/2016JF004181

MacAyeal, D. R. (1989). Large-scale ice flow over viscous basal sediment: Theory and application to Ice Stream B, Antarctica. *Journal of Geophysical Research*, *94*(B4), 4071–4087. https://doi.org/10.1029/JB094iB04p04071

MacAyeal, D. R. (1992). The basal stress distribution of Ice Stream E, Antarctica, inferred by control methods. *Journal of Geophysical Research*, *97*(B1), 595–603. https://doi.org/10.1029/91JB02454

MacAyeal, D. R. (1993). A tutorial on the use of control methods in ice-sheet modeling. *Journal of Glaciology*, *39*(131), 91–98. https://doi.org/10.3198/1993JoG39-131-91-98

Morlighem, M., Rignot, E., Seroussi, H., Larour, E., Ben Dhia, H., & Aubry, D. (2010). Spatial patterns of basal drag inferred using control methods from a full-Stokes and simpler models for Pine Island Glacier, West Antarctica. *Journal of Geophysical Research*, *37*, L14502. https://doi.org/10.1029/2010GL043853

Morlighem, M., Seroussi, H., Larour, E., & Rignot, E. (2013). Inversion of basal friction in Antarctica using exact and incomplete adjoints of a higher-order model. *Journal of Geophysical Research: Earth Surface*, *118*, 1746–1753. https://doi.org/10.1002/jgrf.20125

Petra, N., Zhu, H., Stadler, G., Hughes, T. J. R., & Ghattas, O. (2012). An inexact Gauss-Newton method for inversion of basal sliding and rheology parameters in a nonlinear Stokes ice sheet model. *Journal of Glaciology*, *58*(211), 889–903. https://doi.org/10.3189/2012JoG11J182

Pollard, D., & DeConto, R. M. (2012). A simple inverse method for the distribution of basal sliding coefficients under ice sheets, applied to Antarctica. *The Cryosphere*, *6*, 953–971. https://doi.org/10.5194/tc-6-953-2012

Raymond, M. J., & Gudmundsson, G. H. (2009). Estimating basal properties of ice streams from surface measurements: A nonlinear Bayesian inverse approach applied to synthetic data. *The Cryosphere*, *3*(2), 265–278. https://doi.org/10.5194/tc-3-265-2009

Raymond Pralong, M., & Gudmundsson, G. H. (2011). Bayesian estimation of basal conditions on Rutford Ice Stream, West Antarctica, from surface data. *Journal of Glaciology*, *57*(202), 315–324. https://doi.org/10.3189/002214311796406004

Schoof, C. (2005). The effect of cavitation of glacier sliding. *Proceedings of the Royal Society A*, *461*(2055), 609–627. https://doi.org/10.1098/rspa.2004.1350

Sergienko, O. V., & Hindmarsh, R. C. A. (2013). Regular patterns in frictional resistance of ice-stream beds seen by surface data inversion. *Science*, *342*(6162), 1086–1089. https://doi.org/10.1126/science.1243903

Sergienko, O. V., Bindschadler, R. A., Vornberger, P. L., & Macayeal, D. R. (2008). Ice stream basal conditions from block-wise surface data inversion and simple regression models of ice stream flow: Application to Bindschadler Ice Stream. *Journal of Geophysical Research*, *113*, F04010. https://doi.org/10.1029/2008JF001004

Smith, A. M. (1997). Basal conditions on Rutford Ice Stream, West Antarctica, from seismic observations. *Journal of Geophysical Research*, *102*(B1), 543–552. https://doi.org/10.1029/96JB02933

Smith, A. M. (2007). Subglacial bed properties from normal-incidence seismic reflection data. *Journal of Environmental and Engineering Geophysics*, *12*(1), 3–13. https://doi.org/10.2113/JEEG12.1.3

Smith, A. M., & Murray, T. (2009). Bedform topography and basal conditions beneath a fast-flowing West Antarctic ice stream. *Quaternary Science Reviews*, *28*(7), 584–596. https://doi.org/10.1016/j.quascirev.2008.05.010

Smith, A. M., Jordan, T. A., Ferraccioli, F., & Bingham, R. G. (2013). Influence of subglacial conditions on ice stream dynamics: Seismic and potential field data from Pine Island Glacier, West Antarctica. *Journal of Geophysical Research: Solid Earth*, *118*, 1471–1482. https://doi.org/10.1029/2012JB009582

Smith, E. C., Smith, A. M., White, R. S., Brisbourne, A. M., & Pritchard, H. D. (2015). Mapping the ice-bed interface characteristics of Rutford Ice Stream, West Antarctica, using microseismicity. *Journal of Geophysical Research: Earth Surface*, *120*, 1881–1894. https://doi.org/10.1002/2015JF003587

Taylor, C., & Hood, P. (1973). A numerical solution of the Navier-Stokes equations using the finite element technique. *Computers & Fluids*, *1*(1), 73–100. https://doi.org/10.1016/0045-7930(73)90027-3

Thorsteinsson, T., Raymond, C. F., Gudmundsson, G. H., Bindschadler, R. A., Vornberger, P., & Joughin, I. (2003). Bed topography and lubrication inferred from surface measurements on fast-flowing ice streams. *Journal of Glaciology*, *49*(167), 481–490. https://doi.org/10.3189/172756503781830502

Tulaczyk, S. (2006). Scale independence of till rheology. *Journal of Glaciology*, *52*(178), 377–380. https://doi.org/10.3189/172756506781828601

Tulaczyk, S., Kamb, W. B., & Engelhardt, H. F. (2000). Basal mechanics of Ice Stream B, West Antarctica. 2. Undrained plastic bed model. *Journal of Geophysical Research*, *105*(B1), 483–494. https://doi.org/10.1029/1999JB900328

Vaughan, D. G., Smith, A. M., Nath, P. C., & Le Meur, E. (2003). Acoustic impedance and basal shear stress beneath four Antarctic ice streams. *Annals of Glaciology*, *36*, 225–232. https://doi.org/10.3189/172756403781816437

Vieli, A., & Payne, A. (2003). Application of control methods for modelling the flow of Pine Island Glacier, West Antarctica. *Annals of Glaciology*, *36*(1), 197–204. https://doi.org/10.3189/172756403781816338

Weertman, J. (1957). On the sliding of glaciers. *Journal of Glaciology*, *3*(21), 33–38. https://doi.org/10.1002/2016GL069937